Influence of the sulphurization time on the morphological, chemical, structural and electrical properties of Cu$_2$ZnSnS$_4$ polycrystalline thin films

J.C. González, P.A. Fernandes, G.M. Ribeiro, A. Abelenda, E.R. Viana,
P.M.P. Salomé, A.F. da Cunha

ABSTRACT

The effects of the sulphurization annealing time on the morphological, chemical, structural and electrical properties of CZTS thin films were investigated by scanning electron microscopy, X-ray energy dispersive spectroscopy, Hall effect and electrical conductivity measurements in samples annealed during different time intervals. The increase of the annealing time was found to improve the chemical composition of the samples and to, slightly, increase the crystallite size. Small amounts of Na were measured in the samples. However, the concentration of Na does not increase significantly with the annealing time and should not modify the characteristics of the CZTS thin films. It was also found that at high temperature the electrical conductivity is dominated by thermal emission of carriers over the inter-grain potential barriers. As the temperature decreases different hopping conduction mechanisms start to dominate. At first with nearest-neighbour hopping and successively changing to variable range hopping conduction with a crossover from Mott and Efros–Shklovskii behavior. The electrical conductivity, the concentration of free holes, acceptors and donors, traps' density at the grain boundaries and the grain potential barriers height were found to increase with the annealing time. However, a significant drop in the compensation ratio from 0.8 to 0.5 was also detected.

1. Introduction

Cu$_2$ZnSn(S, Se)$_4$ (CZTSSe) semiconductor compound, is a potential candidate to replace Cu(In,Ga)Se$_2$ (CIGS) as absorber layer in thin film solar cells due in part to its similar physical properties and in other part due to the similarity in the fabrication techniques and solar cell stack [1–5]. In addition, this compound is constituted by inexpensive, earth abundant and non-toxic elements, which opens the possibility of industrial production levels in the range of TW [6]. A recent report of power conversion efficiency exceeding 10% in CZTSSe-based solar cells [7] has increased the interest in this material system and the record stands now at 11.1% [8]. Despite these recent developments, the best conversion efficiency attained so far in pure sulfur CZTS-based solar cell is 8.4% [9]. Chen et al. [10] have suggested that such a low photovoltaic efficiency could be related to difficulties in the synthesis of high quality CZTS absorber layers, since the formation of stoichiometric CZTS has a very narrow chemical potential window. These synthesis problems are more evident considering that the best solar cells are attained using non-stoichiometric absorber layers with compositions poor in Cu [11], i.e. a value of [Cu]/([Zn]+[Sn]) < 1, and rich in Zn, i.e. [Zn]/[Sn] > 1. Todorov et al. [12] have also pointed out that the electrical resistivity of the CZTS could be a limiting factor of the low efficiency of those cells. The properties of the grain boundaries and the passivation of the grain boundaries by high density of acceptors have been proved to play an important role in the high conversion efficiency of CIGS-based solar cells [13–15]. Nonetheless, the nature of the electrical conduction mechanisms, the density of acceptors and donors impurities and the role of the grain boundaries have not been studied in enough detail in polycrystalline CZTS thin films and solar cells [3,4,16–20]. The understanding of these properties is of absolute importance for the optimization of the material and also of the structure of the solar cell devices.

In this work, a study of the direct current (DC) electrical transport properties of CZTS thin layers grown by sequential deposition of metallic precursors, followed by thermal annealing

in sulfur atmosphere during different time intervals, is presented. Firstly, a morphological, chemical and structural study of the CZTS layers will be presented in order to have a large picture of the effects of the annealing time over the physical properties of such material. Secondly, a wavelength dispersive X-ray spectroscopy study of the limited diffusion of Na into the CZTS films will be presented. Finally, the investigation of the electrical transport properties of the CZTS layers as a function of temperature will be presented. In addition the influence of the sulphurization annealing time over several parameters will also be discussed.

2. Materials and methods

2.1. Sample preparation

CZTS thin films were grown following the procedure reported elsewhere [3,4,18,19]. Soda lime glass (SGL) substrates of 3×3 cm^2 were sequentially cleaned in ultrasound baths of acetone, ethanol and deionized water (DI), and subsequently dried with a N$_2$ flow. Next, thin metallic layers of Zn, Sn and Cu were sequentially deposited over the SLG substrate by dc-magnetron sputtering. All depositions were done in Ar atmosphere at an operating pressure of 2×10^{-3} mbar. Power densities of 0.16, 0.36 and 0.11 Wcm^{-2} were used for Cu, Zn and Sn deposition, respectively. The distance between the target and the samples was kept at 8 cm. The purity of the targets was 5 N for Cu and 4 N for both Zn and Sn. After the deposition of the metallic thin layers, the samples were annealed in a tubular furnace under a sulfur atmosphere. Sulfur was evaporated from 5 N purity pellets at 130 °C in a temperature controlled quartz tube source. Dry N$_2$ at a constant 5 mbar pressure and a flow rate of 40 ml/min was used as a carrier gas. The furnace temperature was increased at constant rate of 10 °C/min until 520 °C. The temperatures were kept constant at 520 °C during the annealing time, and then the furnace was left to cool down naturally. Three different samples A10, A30 and A90 were prepared with annealing times of 10 min, 30 min and 90 min, respectively.

After the thermal annealing, unwanted Cu$_{2-x}$S phases that are formed during the CZTS crystallization process were removed by a wet etching in a KCN solution at 10% w/w, followed by cleaning in a solution of ethanol/DI water at 50% vol/vol and finally rinsed with DI water. Each step had duration of 2 min. Finally, all samples were dried with a N$_2$ gas flux.

In other to carry out accurate electrical transport measurements and to avoid any possible influence of the MoS$_x$ layer formed at the Mo/CZTS interface [18], the thin films studied were deposited on bare SLG substrates. However, as will be shown the physical and chemical properties of these films are not significantly changed by the lack of the Mo layer.

2.2. Sample characterization

The morphology and chemical composition of the samples was studied by using scanning electron microscopy (SEM – Hitachi S4100 SEM®) and X-ray energy dispersive spectroscopy (EDS). X-ray wavelength dispersive spectroscopy (WDS) was used to study the incorporation of sodium (Na) from the SLG substrates into the CZTS thin films. X-ray diffraction (XRD – PHILIPS PW 3710 system®) was used for the structural characterization and the identification of the crystallographic phases present in the samples.

The electrical measurements in the present study are based on DC in-plane transport probing a large number of grains and grain boundaries. The electrical transport properties of the samples were studied by carrying out DC Hall effect measurements at room temperature, and electrical resistivity measurements, in darkness, as a function of temperature in the range of 10–310 K.

For these measurements, four square gold contacts of 1 mm^2 size were deposited at the corners of 6×6 mm^2 CZTS thin films samples. The measurements were carried out by the Van der Pauw method. The samples were mounted in an Oxford Instrument Spectrostat® static continuous flow cryostat CF104®, especially modified for very low noise electrical measurements. The cryostat was controlled by an Oxford Instrument ITC503® temperature controller. The electrical measurements were done with a homemade low noise setup.

3. Results and discussion

3.1. Morphological characterization

Fig. 1 shows the surface of the CZTS thin films as measured by SEM. The samples are polycrystalline with a very similar morphology and a few voids, caused by the KCN etching. The average grain size, s, and grain size dispersion, Δs, reported here as $(s \pm \Delta s)$ was determined from several SEM images as (0.36 ± 0.24) μm, (0.43 ± 0.21) μm, and (0.44 ± 0.22) μm for samples A10, A30 and A90, respectively. A small increase in the average grain size with the annealing time can be observed. However, the grain size dispersion remains approximately constant indicating an improvement of the grain size homogeneity ($\Delta s/s$) with the annealing time.

3.2. Chemical composition

The chemical composition of the samples was analyzed by EDS. The electron beam energy used in the EDS experiments was of 25 keV, meaning that the X-ray generation range in CZTS is larger than 1.8 μm and covers the whole thickness of the CZTS thin films ($\sim$1.6 μm). A summary of the EDS analysis is shown in Table 1, presenting the elemental atomic percentage and composition ratios. All samples are off-stoichiometry, with low concentration of Cu, as intended. The increase in the annealing time slightly improves the stoichiometry of the samples by increasing the composition of Cu and by reducing the composition of Zn.
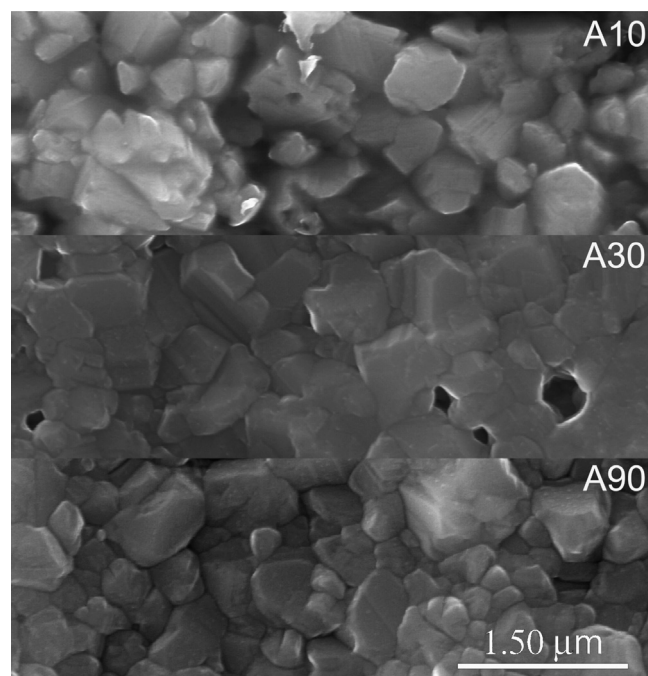

Fig. 1. SEM image of the surface of the CZTS samples A10, A30 and A90.

Table 1

Atomic percentage (at%) and composition ratios ([x]/[y]) for metallic elements as measured by EDS.

Sample	Cu(%)	Zn(%)	Sn(%)	[Cu]/([Zn]+[Sn])	[Zn]/[Sn]	[Cu]/[Zn]	[Cu]/[Sn]	[S]/([Cu]+[Zn]+[Sn])
A10	22 ± 3	18 ± 3	11 ± 2	0.8 ± 0.2	1.6 ± 0.6	1.2 ± 0.3	2.0 ± 0.6	1.0 ± 0.3
A30	23 ± 3	12 ± 2	13 ± 2	0.9 ± 0.3	0.9 ± 0.3	1.9 ± 0.6	1.8 ± 0.5	1.0 ± 0.3
A90	24 ± 3	13 ± 2	12 ± 2	0.9 ± 0.3	1.1 ± 0.3	1.8 ± 0.5	2.0 ± 0.6	1.0 ± 0.3
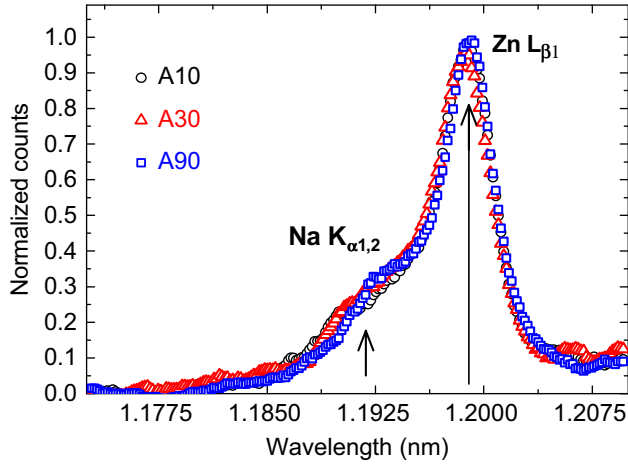
Fig. 2. WDS spectra of the Na $K_{\alpha1,2}$ and Zn $L_{\beta1}$ lines for the CZTS samples A10, A30 and A90.

Fig. 3. XRD difractograms of the CZTS samples A10, A30 and A90. The CZTS peaks have been identified by their orientation plane assignments.

The incorporation of significant amounts of Na is known to modify the morphological and electrical properties of CZTS thin films [21–23]. The Na diffusion from the SLG substrate into the CZTS thin film could be enhanced by the increase in the annealing time of the sample, and consequently, also be responsible for modifications of the electrical properties of the films. The presence of Na cannot be detected by EDS, due to the limited energy resolution of this technique that results in the overlapping of the Na K lines and the strong Zn L lines. However, by using WDS it is possible to resolve these lines. Fig. 2 shows the WDS spectra of Na $K_{\alpha1,2}$ and Zn $L_{\beta1}$ lines for the three samples studied here. The spectra have been normalized in order to clearly show that the amount of Na is not increasing with the annealing time. We estimated the amount of Na around 0.08 at% in these samples. For similar CZTS thin films, but deposited on Mo covered SLG substrates, we have found similar amounts of Na with values between 0.08 at% and 0.12 at%. The electron beam energy used in the WDS experiments was of 10 keV, meaning that the X-ray generation range in CZTS is shorter than thickness of the CZTS thin films, in order to avoid the excitation of the Na atoms in the SLG substrate. Until the present date there are no studies about the optimum amount of Na for CZTS-based solar cells. However, since CIGS and CZTS appear to share some properties, it is important to point out that for CIGS-based solar cells 0.1 at% of Na has been found to optimize the performance of the cells [24–27]. Therefore, we understand that the properties of the CZTS samples of this study are comparable to properties of CZTS grown on Mo.

3.3. Structural characterization

The structural analysis and the phase identification were carried out by XRD. Fig. 3 shows the XRD diffractograms of the samples. The samples were found to be made of polycrystalline CZTS. The average crystallites size was calculated from the full width at half maximum (FWHM) of the XRD peaks, according to Scherrer´s equation [28]. The FWHM of the (112) peaks were
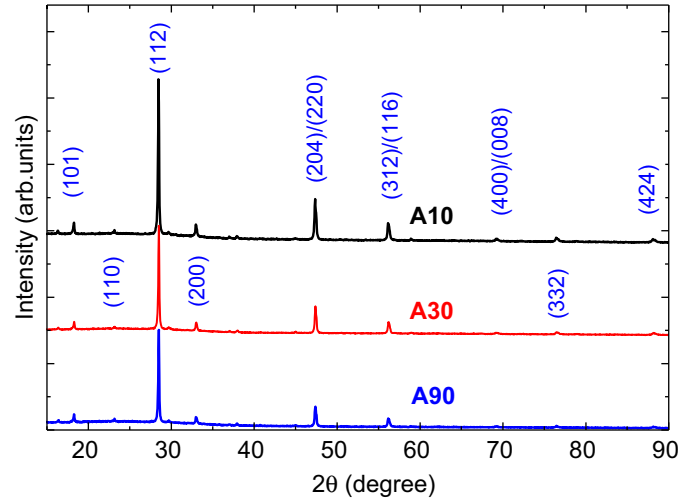
Table 2

Results of the Hall effect measurements at 300 K.

Sample	ρ (Ω cm)	p_{Hall} (10^{17} cm^{-3})	μ_{Hall} (cm^2/V s)
A10	25.1	1.0	2.5
A30	19.4	1.5	2.1
A90	3.9	27.8	0.58

determined as 0.185°, 0.180° and 0.176° for samples A10, A30 and A90, respectively. In order to determine the crystallite size, instrument´s peak broadening of 0.148° was used. The crystallite sizes were found to slightly increase with the annealing time, with values of 120 nm for sample A10, 130 nm of sample A30 and 140 nm for sample A90. Since the mean grain size found in the SEM studies is several times larger than the average crystallite sizes we believe that the grains observed by SEM actually contain more than one crystallite.

3.4. Electrical characterization

Hall effect measurements were carried out at near room temperature. However, due to the low values of the Hall mobility and high values of Hall carriers' concentration it was not possible to obtain reproducible values of these parameters for lower temperatures. The measured values of the Hall mobility and concentration of carriers are summarized in Table 2. All measured samples were found to exhibit p-type conductivity. A clear increase of the Hall concentration, p_{Hall}, was observed as the annealing time increases. However, the Hall mobility, μ_{Hall}, decreased with the annealing time.

The temperature dependence of the electrical resistivity, $\rho(T)$, of the samples is shown in Fig. 4. Two regimes are observed in
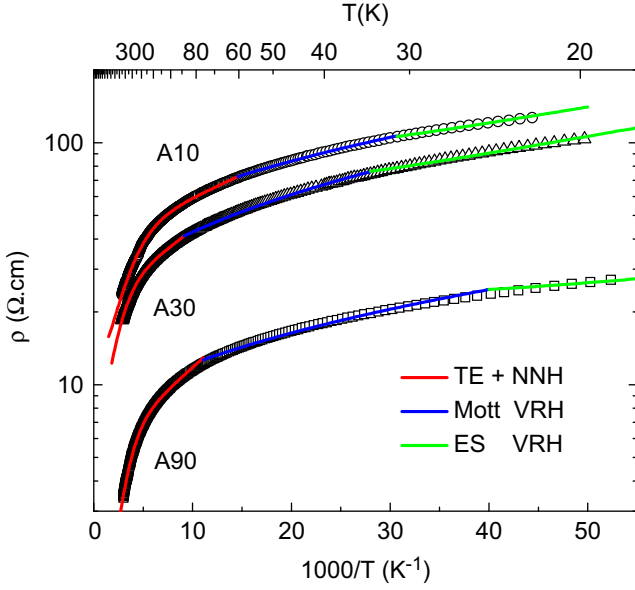
Fig. 4. Temperature dependence of the electrical resistivity of the CZTS samples A10, A30 and A90. The solid lines are the fitting of the experimental data using Eqs. (1) (TE), (3) (NNH), (5) (Mott-VRH) and (9) (ES-VRH) (For interpretation of the references to color in the text, the reader is referred to the web version of this article).

those curves. At high temperatures, $\rho(T)$ exhibits an Arrhenius like behavior, while notably deviates from it at lower temperatures.

At high temperatures the electrical conduction of polycrystalline thin films is dominated by thermionic emission of carriers over the inter-grain potential barriers (GPB) [19]. The temperature dependence of the electrical resistivity of the p-type polycrystalline thin film can then be expressed as [29]

$$\rho_{TE}(T) = \rho_0 \sqrt{T} \exp(\phi/k_B T) \qquad (1)$$

where ρ_0 is a constant, k_B is Boltzmann´s constant and the exponential factor describes the thermal activation of carriers' mobility flowing over the GPB with height ϕ. The GPB height can be related to the doping level p, the dielectric permittivity ε [30], and traps' density N_t at the grain boundary according to [31]

$$\phi = \left(e^2 N_t^2\right)/(8\varepsilon p) \qquad (2)$$

However, as temperature decreases, holes do not have sufficient thermal energy to be excited from the acceptor levels to the valence band [32] and the conduction in the valence band becomes less important. In this case, holes can hop between nearest-neighbour acceptors in the impurity band. The Nearest-Neighbour hopping conduction (NNH) becomes the main conduction mechanism [32,33]. The resistivity of NNH is given by [32]

$$\rho_{NNH}(T) = \rho_1 \exp(E_{NNH}/k_B T) \qquad (3)$$

$$E_{NNH} = \left(0.99\, e^2 N_A^{1/3}\right)/(4\pi\varepsilon) \qquad (4)$$

where ρ_1 is a constant, N_A is the concentration of acceptors and E_{NNH} is the activation energy for hole hopping.

Both conduction mechanisms, thermionic emission and NNH, are present in the high temperature range of the data ($T \gtrsim 90$ K, $1000/T \lesssim 11.11$ K^{-1}). Therefore, it is possible to extract some of the above mentioned parameters by fitting of the resistivity data with $\rho(T) = \rho_{TE}(T)\rho_{NNH}(T)/[\rho_{TE}(T) + \rho_{NNH}(T)]$. The fitting of this expression for each sample is shown, by solid red lines, in Fig. 4. These mechanisms explain well our high temperature data. The results of the fittings are shown in Table 3.

Table 3
Parameters of the thermionic emission and NNH conduction in the samples.

Sample	ρ_o (Ω cm K$^{-1/2}$)	ρ_1 (Ω cm)	ϕ (meV)	E_{NNH} (meV)	N_A (10^{15} cm^{-3})	N_t (10^{11} cm^{-2})
A10	322.5	38.6	64.4	3.7	5.4	3.9
A30	150.4	21.7	92.5	6.0	22.6	11.2
A90	12.1	5.1	101.2	7.2	39.6	30.8

Tables 2 and 3 show a decrease of the resistivity and hole mobility as the annealing time increases, while holes' concentration, the density of acceptors and traps' density at the grain boundaries increase. The reduction of the hole mobility is associated with the increase of the GPB height. A similar increase in the GPB with the annealing time was observed in CZTS polycrystalline thin films by Kosyak et al. [34].

At lower temperatures the resistivity data can be explained in terms of variable-range hopping conduction (VRH). VRH was originally developed by Mott [35], pointing out that the energy difference ΔE between the initial and final sites involved in the hopping is related to the hopping distance r as $\Delta E \sim 1/N_0(E_F)r^3$, if there is a constant density of states (DOS), $N_0(E_F)$, near the Fermi level. The resistivity of the Mott VRH conduction mechanism is given by [35]

$$\rho_M(T) = \rho_{0M} T^{1/2} \exp\left[\left(T_M/T\right)^{1/4}\right] \qquad (5)$$

where ρ_{0M} is a pre-exponential factor and T_M measures the degree of disorder in the film. The characteristic temperature T_M is given by

$$T_M = \alpha/\left(k_B N_0(E_F)\xi^3\right) \qquad (6)$$

where the constant $\alpha = 18.1$, and ξ is the localization length, which characterizes the hopping probability between both sites.

In disordered or highly compensated materials the transition from NNH conduction to Mott-VRH conduction occurs at a critical temperature T_{CM}. This critical temperature was theoretically described by Shklovskii [36] for samples with compensation ratios k larger than 0.5 as

$$T_{CM} = \left(e^2 N_A^{2/3} \xi\right)/(4\pi\varepsilon k_B) \qquad (7)$$

Furthermore, the compensation ratio, for $k > 0.5$, can be calculated from [36]

$$k = N_D/N_A = 1 - \left(N_0 E_F e^2/2\varepsilon\right)^{3/4}\left(1/N_A\right)^{1/2} \qquad (8)$$

The $T^{1/4}$ Mott's Law has been observed in various classes of doped semiconductors. Nevertheless, a large body of literature reported $T^{1/2}$ at low temperatures instead of Mott's. Efros and Shklovskii [36] argued that at low temperatures the Coulomb interaction would open a soft gap Δ in the DOS. Therefore, if the temperature decreases below a crossover value T_C such that $k_B T_C < \Delta$, the Coulomb effect becomes dominant and the conductivity crosses over from Mott-VRH to ES-VRH regime. The resistivity in the ES-VRH regime is given by

$$\rho_{ES}(T) = \rho_{0ES} T \exp\left(\left(T_{ES}/T\right)^{1/2}\right) \qquad (9)$$

$$T_{ES} = (\beta e^2)/(\varepsilon k_B \xi) \qquad (10)$$

where $\beta = 2.8$ and the pre-exponential factor ρ_{0ES} is a proportionality constant.

The characteristic temperatures T_M and T_{ES} can be obtained by fitting the resistivity data with Eqs. (5) and (9). The hopping parameters, as well as the compensation ratio, can then be obtained from Eqs. (6)–(10). Fig. 5 shows the fitting of the

resistivity data using Eqs. (5) and (9). The values of the hopping parameters, the compensation ratio, the crossover T_C and critical T_{CM} temperatures are reported in Table 4.

Table 4 shows a significant decrease of the compensation ratio for the sample with the longest annealing time, A90. However, the compensation ratio is still high for these samples. Acceptors' and donors' concentration also increased with the annealing time. The large compensation ratio, as well as the elevated concentration of donors and acceptors, leads to an enhancement of the disorder in the samples [37]. Previous photoluminescence and photoconductivity studies [3,4,19] revealed that these characteristics produce local potential fluctuations in CZTS thin films.

It is now important to discuss the possible role of the Na incorporation in the samples as the annealing time increases, since Na might have an important role in the electronic behavior of the material. As mentioned before, the intentional addition of Na during the CZTS deposition increases: the grain size [22,23], free carriers' concentration and the electrical conductivity [23]. The effects of the incorporation of Na on the electrical properties of CZTS are similar to the case of CIGS, with an increase in free carriers' concentration due to a lower number of compensating donors [38]. The addition of Na is also known to enhance the cells performance by improving the open-circuit voltage, fill factor, short-circuit current and efficiency of the cells [24,39]. However, the Na dose must be optimized, because an excessive or insufficient doping produces a detrimental effect on the cell performance [40,41]. A recent report [23] showed that the Na diffusion into CZTS depends of the Mo layer deposition conditions and that the Na concentration in CZTS layers deposited on Mo covered SLG substrates can be as large as in the case of CZTS layers deposited directly on SLG substrates.

The samples studied here present a similar Na concentration to that of CZTS thin film deposited on Mo-covered SLG substrates,
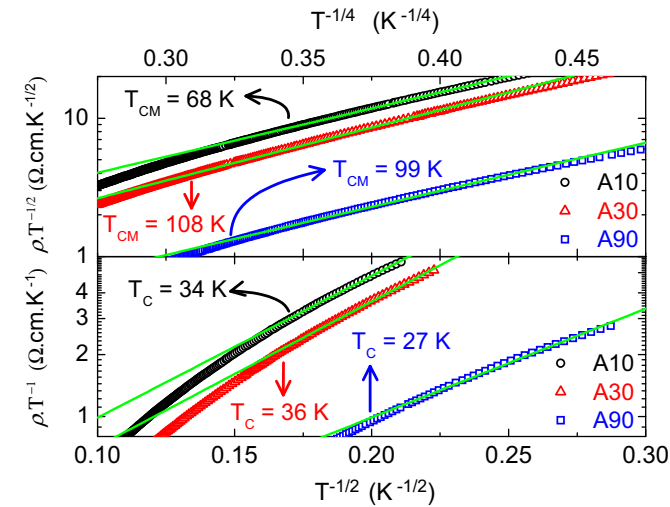
and it does not increase with the annealing time. However, free holes' concentration, acceptors' concentration and the electrical conductivity increase with annealing time. The compensation ratio in the samples is high, but decreases significantly for the sample with the longest annealing time. All of these mentioned characteristics could be associated with the incorporation of Na into the CZTS thin films. However, donors' concentration increases, in contradiction with the expected effects of significant Na incorporation in CZTS. The crystallites and grain sizes measured by XRD and SEM suffer just a slight increase, likewise in opposition to the expectation from a significant incorporation of Na into the films. Therefore, as far as our experimental data indicates, the Na concentration in the samples is low and similar to the concentration found in CZTS films deposited on Mo-covered SLG substrates. It is our interpretation that the observed changes in the morphological and electrical characteristics of the samples are actually due to effects connected with the increase of the annealing time and not to the ones related to the incorporation of Na in the samples. These results strongly support the idea that electrical transport measurements in CZTS thin films grown on SLG are a valuable method to study the electrical properties and parameters of the actual CZTS absorber layers of the solar cells deposited on Mo-covered SLG substrates.

In a recent work [20], we studied the effects of the sulphurization time on the alternated current (ac) electrical properties of CZTS solar cells by admittance spectroscopy. The study shows a deterioration of the main parameters of the cell (open-circuit voltage, saturation current, fill factor and efficiency) with the increase of the sulphurization time. However, other parameters such as the serial and shunt resistances remain constant or actually decrease. The concentration of majority carrier was also found to decrease. The apparent contradiction with the results of this work has to be explained in the light of the fact that we are comparing two very different techniques. Admittance spectroscopy is a technique that mostly measures transport in the vertical direction of the solar cell stack and probes a few grains and grain boundaries, while the electrical measurements in the present study are based on DC in-plane transport probing a large number of grains and grain boundaries.

This antagonist behavior between AC/DC measurements can also relay on the differences that the samples present, when comparing the sets of samples grown with and without the Mo back contact. In addition, the absorber layer electronic properties are influenced by the presence of the other layers that composes the solar cell structure. In particular, the conjugated influence of the CdS buffer layer, which forms the p–n heterojunction with the CZTS and the MoS_2 layer, which in turn forms an inverted diode with the CZTS, are not entire understood and need further research work clarify these behaviors and to allow a direct comparison between AC and DC analysis.

The variation of the chemical composition of the samples could be responsible for the changes observed in the electrical properties. It should be noted that our samples are poor in Cu and rich in Zn, particularly sample A10. Copper vacancies form shallow acceptors [42]. On the other hand Zn related point defects, such as interstitial Zn and ZnCu anti-sites, form donor defects [42].

Fig. 5. Temperature dependence of the resistivity of the CZTS samples A10, A30 and A90, in the Mott-VRH and ES-VRH regimes. The solid lines in (a) and (b) correspond to the linear fitting with Eqs. (5) and (9), respectively.

Table 4
Parameters of the Mott- and ES-VRH conduction.

Sample	ρ_{0M} (Ω cm K$^{-1/2}$)	ρ_{0ES} (Ω cm K^{-1})	T_M (K)	T_{ES} (K)	T_C (K)	T_{CM} (K)	k	N_D (10^{15} cm^{-3})
A10	213.1	201.7	13,086	252.3	34	68	0.82	4.4
A30	104.0	141.2	19,107	263.3	36	108	0.80	18.1
A90	34.0	86.4	15,904	148.6	27	99	0.51	20.2

These defects could be responsible for the high doping levels and large degree of compensation in the samples, particularly in sample A10. The increase of the sulphurization time improves the stoichiometry of the samples, probably reducing the Zn related point defects and explaining the decrease in the compensation of the samples. However, it is very difficult to establish a direct relationship between chemical and electrical properties in polycrystalline thin films due to the complexity of the electrical transport mechanism in those films.

4. Conclusions

The morphology, chemical composition and electrical conductivity properties of polycrystalline CZTS thin films sulphurized during different periods of time were investigated. The increase of the sulphurization annealing time was found to increase slightly the average grain and crystallite size of the polycrystalline CZTS thin films. The thin films were found to be off-stoichiometry, that is, poor in Cu and rich in Zn. The concentration of Na in the samples was found to be approximately 0.08 at% and independent of the annealing time. The analysis of Hall effect and electrical resistivity measurements show that the CZTS thin films are p-type and highly doped. It was found that at temperatures higher than approximately 90 K the electrical conductivity of the samples is dominated by thermoionic emission and nearest-neighbour hopping conduction. However, at lower temperatures both, Mott- and ES-VRH were observed. A crossover from Mott- to ES-VRH regime was determined at approximately 30 K. The analysis of the electrical transport shows that an increase on the annealing time increases free holes' concentration in the samples as well as the concentration of acceptors and donors. The compensation ratio decreases from approximately 0.8 for the samples annealed between 10 and 30 min, to 0.5 for the sample annealed during 90 min. An increase of traps' density at the grain boundaries and the GPB height, that produces a drop in the free hole mobility, was also observed. The observed changes in the morphological and electrical characteristics of the samples were found to be actually due to the increase of the annealing time and not to the incorporation of sodium in the samples. These results could contribute for a better optimization of not only the CZTS absorber layer, but also for the choice of the materials used in the solar cell stack.

References

[1] P.M.P. Salomé, J. Malaquias, P.A. Fernandes, M.S. Ferreira, A.F. da Cunha, J.P. Leitão, J.C. González, F.M. Matinaga, Growth and characterization of $Cu_2ZnSn(S,Se)_4$ thin films for solar cells, Sol. Energy Mater. Sol. Cells 101 (2012) 147–153.

[2] P.M.P. Salomé, P.A. Fernandes, A.F. da Cunha, J.P. Leitão, J. Malaquias, A. Weber, J.C. González, M.I.N. da Silva, Growth pressure dependence of $Cu_2ZnSnSe_4$ properties, Sol. Energy Mater. Sol. Cells 94 (2010) 2176–2180.

[3] J.P. Leitão, N.M. Santos, P.A. Fernandes, P.M.P. Salomé, A.F. da Cunha, J.C. González, G.M. Ribeiro, F.M. Matinaga, Photoluminescence and electrical study of fluctuating potentials in Cu_2ZnSnS_4-based thin films, Phys. Rev. B 84 (2011) 024120–024128.

[4] J.P. Leitão, N.M. Santos, P.A. Fernandes, P.M.P. Salomé, A.F. da Cunha, J.C. González, F.M. Matinaga, Study of optical and structural properties of Cu_2ZnSnS_4 thin films, Thin Solid Films 519 (2011) 7390–7393.

[5] P.M.P. Salomé, J. Malaquias, P.A. Fernandes, M.S. Ferreira, J.P. Leitão, A.F. da Cunha, J.C. González, F.M. Matinaga, G.M. Ribeiro, E.R. Viana, The influence of hydrogen in the incorporation of Zn during the growth of Cu_2ZnSnS_4 thin films, Sol. Energy Mater. Sol. Cells 95 (2011) 1–4.

[6] V.M. Fthenakis, Sustainability of photovoltaics: the case for thin film solar cells, Renew. Sustain. Energy Rev. 13 (2009) 2746–2750.

[7] D. Aaron, R. Barkhouse, O. Gunawan, T. Gokmen, T.K. Todorov, D.B. Mitzi, Device characteristics of a 10.1% hydrazine-processed $Cu_2ZnSn(Se,S)_4$ solar cell, Prog. Photovolt. Res. Appl. 20 (2012) 6–11.

[8] T.K. Todorov, J. Tang, S. Bag, O. Gunawan, T. Gokmen, Y. Zhu, D.B. Mitzi, Beyond 11% efficiency: characteristics of state-of-the-art $Cu_2ZnSn(S,Se)_4$ solar cells, Adv. Energy Mater. 3 (2013) 34–38.

[9] H. Katagiri, K. Jimbo, S. Yamada, T. Kamimura, W.S. Maw, T. Fukano, T. Ito, T. Motohiro, Enhanced conversion efficiencies of Cu_2ZnSnS_4-based thin film solar cells by using preferential etching technique, Appl. Phys. Express 1 (2008) 041201–041202.

[10] S. Chen, X.G. Gong, A. Walsh, S.H. Wei, Defect physics of the kesterite thin-film solar cell absorber Cu_2ZnSnS_4, Appl. Phys. Lett. 96 (2010) 021902–021903.

[11] H. Katagiri, K. Jimbo, M. Tahara, H. Araki, K. Oishi, The influence of the composition ratio on CZTS-based thin film solar cells, in: A. Yamada, C. Heske, M. Contreras, M. Igalson, S.J.C. Irvine (Eds.), Thin-Film Compound Semiconductor Photovoltaics 2009, Materials Research Society Symposium Proceedings, vol. 1165, San Francisco, USA, April 13–17, 2009, pp. 1165-M04–01.

[12] T.K. Todorov, K.B. Reuter, D.B. Mitzi, High-efficiency solar cell with earth-abundant liquid-processed absorber, Adv. Mater. 22 (2010) E156–E159.

[13] M. Gloeckler, J.R. Sites, W.K. Metzger, Grain-boundary recombination in Cu(In, Ga)Se_2 solar cells, J. Appl. Phys. 98 (2005) 113704–113710.

[14] K. Taretto, U. Rau, Numerical simulation of carrier collection and recombination at grain boundaries in Cu(In,Ga)Se_2 solar cells, J. Appl. Phys. 103 (2008) 094523-1–094523-11.

[15] Y. Yan, K.M. Jones, C.S. Jiang, X.Z. Wu, R. Noufi, M.M. Al-Jassim, Understanding the defect physics in polycrystalline photovoltaic materials, Physica B 401–402 (2007) 25–32.

[16] J.B. Li, V. Chawla, B. Clemens, Investigating the role of grain boundaries in CZTS and CZTSSe thin film solar cells with scanning probe microscopy, Adv. Mater. 24 (2012) 720–723.

[17] M.J. Romero, H. Du, G. Teeter, Y. Yan, M.M. Al-Jassim, Comparative study of the luminescence and intrinsic point defects in the kesterite Cu_2ZnSnS_4 and chalcopyrite Cu(In,Ga)Se_2 thin films used in photovoltaic applications, Phys. Rev. B 84 (2011) 165324–165325.

[18] P.A. Fernandes, A.F. Sartori, P.M.P. Salomé, J. Malaquias, A.F. da Cunha, M.P.F. Graça, J.C. González, Admittance spectroscopy of Cu_2ZnSnS_4 based thin film solar cells, Appl. Phys. Lett. 100 (2012) 233504-4.

[19] J.C. González, G.M. Ribeiro, E.R. Viana, P.A. Fernandes, P.M.P. Salomé, K. Gutiérrez, A. Abelenda, F.M. Matinaga, J.P. Leitão, A.F. da Cunha, Hopping conduction and persistent photoconductivity in Cu_2ZnSnS_4 thin films, J. Phys. D Appl. Phys. 46 (2013) 155107-7.

[20] P.A. Fernandes, P.M.P. Salomé, A.F. Sartori, J. Malaquias, A.F. da Cunha, Björn-Arvid Schubert, J.C. González, G.M. Ribeiro, Effects of sulphurization time on Cu_2ZnSnS_4 absorbers and thin films solar cells obtained from metallic precursors, Sol. Energy Mater. Sol. Cells 115 (2013) 157–165.

[21] J.H. Yoon, et al., Optical analysis of the microstructure of a Mo back contact for Cu(In,Ga)Se_2 solar cells and its effects on Mo Film properties and Na diffusivity, Sol. Energy Mater. Sol. Cells 95 (2011) 2959–2964.

[22] W.M. Hlaing, et al., Grain size and texture of Cu_2ZnSnS_4 thin films synthesized by cosputtering binary sulfides and annealing: effects of processing conditions and sodium, J. Electron. Mater. 40 (2011) 2214–2221.

[23] T. Prabhakar, N. Jampana, Effect of sodium diffusion on the structural and electrical properties of Cu_2ZnSnS_4 thin films, Sol. Energy Mater. Sol. Cells 95 (2011) 1001–1004.

[24] D. Rudmann, A.F. da Cunha, M. Kaelin, F. Kurdesau, H. Zogg, A.N. Tiwari, Efficiency enhancement of Cu(In,Ga)Se_2 solar cells due to post-deposition Na incorporation, Appl. Phys. Lett. 84 (2004) 1129–1131.

[25] D. Rudmann, G. Bilger, M. Kaelin, F.-J. Haug, H. Zogg, A.N. Tiwari, Effects of NaF coevaporation on structural properties of Cu(In,Ga)Se_2 thin films, Thin Solid Films 431–432 (2003) 37–40.

[26] P.M.P. Salomé, A. Hultqvist, V. Fjällström, M. Edoff, B. Aitken, K. Vaidyanathan, K. Zhang, K. Fuller, C. Kosik Williams, Cu(In,Ga)Se_2 solar cells with varying Na content prepared on nominally alkali-free glass substrates. IEEE J. Photovolt. 3 (2013) 852–858.

[27] Raquel Caballero, Christian A. Kaufmann, Tobias Eisenbarth, Thomas Unold, Susan Schorr, Raik Hesse, Reiner Klenk, Hans-Werner Schock, The effect of NaF precursors on low temperature growth of CIGS thin film solar cells on polyimide substrates, Phys. Status Solidi A 206 (2009) 1049–1053.

[28] A. Patterson, The Scherrer formula for X-ray particle size determination, Phys. Rev. 56 (1939) 978–982.

[29] R.H. Bube, Electronic transport in polycrystalline films, Annu. Rev. Mater. Sci. 5 (1975) 201–224.

[30] C. Persson, Electronic and optical properties of Cu_2ZnSnS_4 and $Cu_2ZnSnSe_4$, J. Appl. Phys. 107 (2010) 053710–053718.

[31] J.Y.W. Seto, The electrical properties of polycrystalline silicon films, J. Appl. Phys. 46 (1975) 5247–5254.

[32] E.R. Viana, J.C. González, G.M. Ribeiro, A.G. de Oliveira, 3D hopping conduction in SnO_2 nanobelts, Phys. Status Solidi (RRL) 6 (2012) 262–264.

[33] B.I. Shklovskii, Hopping conduction in lightly doped semiconductors, Fiz. Tekh. Poluprov. 6 (1972) 1197 (English transl.: Sov. Phys. Semicond. 6 (1973) 1053-1075.

[34] V. Kosyak, M.A. Karmarkar, M.A. Scarpulla, Temperature dependent conductivity of polycrystalline Cu_2ZnSnS_4 thin films, Appl. Phys. Lett. 100 (2012) 263903–263905.

[35] N.F. Mott, E.A. Davis, Electronic Processes in Non-Crystalline Materials, Clarendon Press, Belfast, Oxford, 1979 (Chapter 2) pp 7-64.

[36] A.L. Efros, B.I. Shklovskii., Electronic Properties of Doped Semiconductors, Springer, Berlin, 1984 (Chapter 9) pp 202-227.

[37] M. Pollak, M. Ortuño., Electron–Electron Interactions in Disordered Systems, North-Holland, Amsterdam, 1985 (Chapter 4) pp 287-408.

[38] D.J. Schroeder, A.A. Rockett, Electronic effects of sodium in epitaxial $CuIn_{1-x}Ga_xSe_2$, J. Appl. Phys. 82 (1997) 4982–4985.

[39] D. Rudmann, D. Brémaud, H. Zogg, A.N. Tiwari, Na incorporation into Cu(In,Ga)Se_2 for high-efficiency flexible solar cells on polymer foils, J. Appl. Phys. 97 (2005) 084903–084905.

[40] P.M.P. Salomé, V. Fjallstrom, A. Hultqvist, P. Szaniawski, U. Zimmermann, M. Edoff., The effect of Mo back contact ageing on Cu(In,Ga)Se_2 thin-film solar cells, Prog. Photovolt. Res. Appl. 22 (2013) 83–89.

[41] R. Caballero, C. Guillén, Structural and morphological properties of Cu(In,Ga)Se_2 thin films on Mo substrate, Appl. Surf. Sci. 238 (2004) 180–183.

[42] Shiyou Chen, Ji-Hui Yang, X.G. Gong, Aron Walsh, Su-Huai Wei, Intrinsic point defects and complexes in the quaternary kesterite semiconductor Cu_2ZnSnS_4, Phys. Rev. B 81 (2010) 245204–245210.